Time-of-flight (TOF) implementation for PET reconstruction in practice

Marina Filipovic, Claude Comtat, Simon Stute

Physics in Medicine & Biology

NOTE • **OPEN ACCESS**

Time-of-flight (TOF) implementation for PET reconstruction in practice

IOP Publishing Phys. Med. Biol. 64 (2019) 23NT01 (8pp) https://doi.org/10.1088/1361-6560/ab4f0b

Physics in Medicine & Biology

IPEM Institute of Physics and Engineering in Medicine

OPEN ACCESS

NOTE

Time-of-flight (TOF) implementation for PET reconstruction in practice

Marina Filipović[1,4], **Claude Comtat**[1] and **Simon Stute**[1,2,3]

[1] Imagerie Moléculaire In Vivo, IMIV, CEA, Inserm, CNRS, University of Paris Sud, Université Paris Saclay, CEA-SHFJ, Orsay, France
[2] Nuclear Medicine Department, University Hospital, Nantes, France
[3] CRCINA, INSERM, CNRS, Université d'Angers, Université de Nantes, Nantes, France
[4] Author to whom any correspondence should be addressed.

E-mail: marina.filipovic.work@gmail.com

Keywords: PET reconstruction, TOF, time-of-flight, implementation, PET/MRI

RECEIVED
4 July 2019

REVISED
25 September 2019

ACCEPTED FOR PUBLICATION
18 October 2019

PUBLISHED
26 November 2019

Abstract

The time-of-flight (TOF) feature of PET scanners has been used for a long time in PET reconstruction, but many implementational aspects are still incomplete or ambiguous in the literature. Here we formalize and present theoretical and practical implementation details for the reconstruction of clinical TOF histogram and list-mode data using ML-EM. Relevant aspects include the computation of the TOF component of the system matrix, the processing of TOF bins, the use of estimations of random and scattered coincidences, and differences between histogram and list-mode ML-EM TOF reconstruction. Several approaches and approximations have been implemented in the CASToR platform and compared for OSEM reconstructions of patient data from the GE Signa PET/MR scanner. Differences between implementations are not larger than the typical bias in clinical data reconstruction. The largest difference and contrast loss occur when the processing of histogram TOF bins is simplified, and list-mode reconstruction is most sensitive to the truncation of the Gaussian TOF probability distribution.

1. Introduction

There is a large amount of literature on different aspects of using time-of-flight (TOF) measurements in PET scanners. However, implementation details for reconstruction algorithms are often incomplete and scattered in various papers dealing either with reconstruction or with related topics (i.e. TOF PET scanners, estimations of random and scattered coincidences). Also, there is no formalization nor comparison of different implementation approaches and approximations. Here we focus on standard quantitative reconstructions from clinical data and on usual primary data formats (list-mode and histogram or raw sinogram), but the considerations are more general and apply to a wide family of algorithms and data formats. The optimization of LOR and TOF binning is not relevant for our purposes and we do not consider the family of TOF reconstruction methods based on preprocessed data formats (i.e. methods performing a single TOF backprojection and iterative operations in the image domain, Snyder and Politte (1983), Matej *et al* (2009)). First, we formalize the implementation of TOF and investigate some details and approximations. For each aspect, we mention articles that provided some theoretical or practical details. Then, we compare several implementations to investigate the impacts of approximations, using the CASToR platform, Merlin *et al* (2018), CAS (2017). This paper is also in support of the implementation of TOF in the CASToR platform.

2. Theory

The TOF measurement for a pair of detected coincident photons is defined as the difference of photon arrival times Δt, but in practice this time difference is converted into v, the presumed spatial position of the annihilation on the LOR. Here v is defined as the position with respect to the center of the LOR, and thus is expressed as $v = \frac{c\Delta t}{2}$, c being the speed of light.

The uncertainty of TOF measurements is usually modelled with a normalized (integral =1) Gaussian function centered at v (Gaussian probability distribution). The Gaussian model and its parameters may be open to consideration because of imperfections of the imaging system, as for instance the spatial inhomogeneity of the timing resolution, the issue of timing alignment, Clementel *et al* (2013), the dependence on the count rate, Levin *et al* (2016), or the accuracy of the estimation of the standard deviation σ, Daube-Witherspoon *et al* (2006).

2.1. Data formats

TOF measurements represent essentially additional information and do not modify other aspects in the acquired data. TOF histogram data contain an additional data matrix dimension for TOF bins: all the counts acquired in a LOR with a certain range of associated TOF measurements are summed into the corresponding TOF bin for that LOR. This implies the sum consistency property: the counts y_{ib} for all TOF bins b in the LOR i must sum to the total counts y_i detected in the LOR,

$$\sum_b y_{ib} = y_i. \tag{1}$$

TOF list-mode data contain an additional TOF measurement value for each detected count, where the measurement can be continuous, though in practice it is necessarily saved with a limited precision, using a certain quantization step.

2.2. Maximum-likelihood expectation-maximization (ML-EM) equations

Let A be the system matrix, λ the radioactive concentration, $\bar{r}$ the expected count rate of random coincidences, $\bar{s}$ the expected count rate of scattered coincidences and j the voxel index. The multiplicative update part u of the ML-EM equation $\lambda_j^{t+1} = u_j^t \lambda_j^t$ for voxel j and iteration t differs for each data format. For TOF histogram data, the measured data are modelled with a Poisson distribution with expectation

$$\bar{y}_{ib} = \sum_j A_{ijb}\lambda_j + \bar{r}_{ib} + \bar{s}_{ib} \tag{2}$$

and thus the update term for histogram data is

$$u_j^t = \frac{1}{\sum_{ib} A_{ijb}} \sum_{ib} A_{ijb} \frac{y_{ib}}{\sum_k A_{ikb}\lambda_k^t + \bar{r}_{ib} + \bar{s}_{ib}}. \tag{3}$$

This equation is used in the papers providing details about TOF histogram reconstruction and in the CASToR platform. The equation for list-mode data with quantized TOF measurements can be derived from the histogram equation (3) as

$$u_j^t = \frac{1}{\sum_{ib} A_{ijb}} \sum_{n=1}^{N_{coinc}} A_{i_n j b_n} \frac{1}{\sum_k A_{i_n k b_n}\lambda_k^t + \bar{r}_{i_n b_n} + \bar{s}_{i_n b_n}}. \tag{4}$$

One could also write an equation for list-mode data with continuous TOF measurements, where the system matrix elements and background contributions are expressed as continuous functions of the TOF measurement v_n,

$$u_j^t = \frac{1}{\sum_{i=1}^{N_{LOR}} \int A_{ij}(v)\mathrm{d}v} \sum_{n=1}^{N_{coinc}} A_{i_n j}(v_n) \frac{1}{\sum_k A_{i_n k}(v_n)\lambda_k^t + \bar{r}_{i_n}(v_n) + \bar{s}_{i_n}(v_n)}. \tag{5}$$

This equation is used in the CASToR version 2. The equation for list-mode data with quantized TOF measurements can also be derived directly from this list-mode equation with continuous TOF measurements (5) as

$$u_j^t = \frac{1}{\sum_{i=1}^{N_{LOR}} \int A_{ij}^q(v)\mathrm{d}v} \sum_{n=1}^{N_{coinc}} A_{i_n j}^q(v_{b_n}) \frac{1}{\sum_k A_{i_n k}^q(v_{b_n})\lambda_k^t + \bar{r}_{i_n}^q(v_{b_n}) + \bar{s}_{i_n}^q(v_{b_n})} \tag{6}$$

without going through the histogram equation (3) (the superscript q stands for 'quantized').

2.3. System matrix elements and TOF weights

Ideally, the system matrix should be modelled by taking into account all the aspects of the acquisition process at once, but in practice it is convenient and reasonably accurate to approximate the system matrix elements as a multiplication of independent terms. Let A_{ij} be the complete explicit system matrix elements for non TOF data, containing the geometric projection and other components. Let w be the TOF weights, independent of A_{ij}, such that the system matrix elements for TOF histogram data are $A_{ijb} = A_{ij}w_{ijb}$, for TOF list-mode data

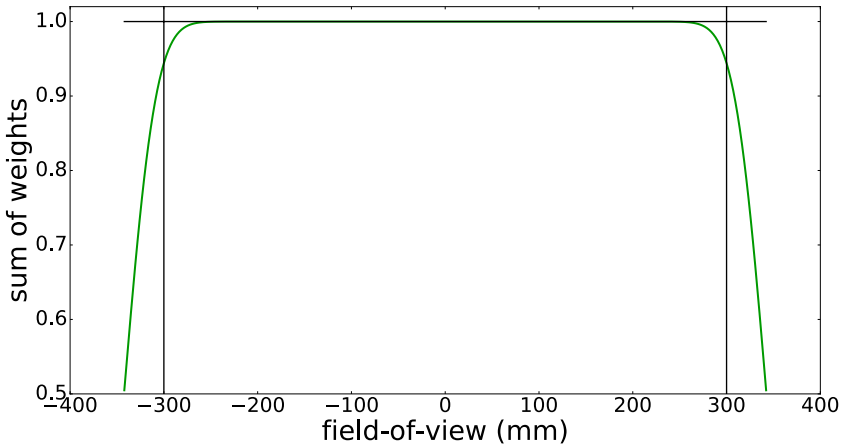

Figure 1. Example of the sum of TOF weights over histogram TOF bins for each voxel along a horizontal LOR passing through the center of the scanner ($\sum_b w_{ijb}$), for the entire transaxial TOF field-of-view (685 mm diameter) of the SIGNA PET/MR scanner; vertical lines show the edges of the largest image field-of-view for reconstruction (600 mm diameter).

with continuous TOF measurements $A_{ij}(\nu) = A_{ij} w_{ij}(\nu)$, and for TOF list-mode data with quantized TOF measurements $A^q_{ij}(\nu_b) = A_{ij} w^q_{ij}(\nu_b)$.

From the sum consistency (1) and from the model (2) follows an important sum consistency property for TOF weights w: the weights for a single LOR, a single voxel, and all TOF bins b or all TOF measurement values ν must sum or integrate to 1, and thus represent a probability distribution.

$$\sum_b w_{ijb} = 1 \quad , \quad \int w_{ij}(\nu)\mathrm{d}\nu = 1 \quad , \quad \int w^q_{ij}(\nu)\mathrm{d}\nu = 1. \tag{7}$$

There is a practical limitation to this property, because of the finite range of TOF measurements. This range can be called the TOF field-of-view and usually matches the size of the coincidence timing window. For voxels close to extreme TOF bins or measurements, the sum/integral (7) decreases. An illustration of this effect is shown in figure 1. The importance of this issue depends on the size of the imaged subject with respect to the scanner. For instance, we may say that the issue becomes of little importance if the distance between the edges of the patient body and of the TOF field-of-view is larger than 3 standard deviations of the TOF uncertainty function (75 mm for the Signa PET/MR). It should be noted that theoretically the sum can never reach exactly 1, because the TOF Gaussian uncertainty function is infinite and the range of TOF measurements finite, but in practice, for instance in the test in figure 1, the sum is equal to 1 in the scanner center.

2.4. Voxel sensitivity

As a consequence of the sum consistency property (7), the voxel sensitivity factors are always the same, regardless of the use of TOF and regardless of the data format (the only paper that mentions this property is Groiselle and Glick (2004)),

$$\sum_i A_{ij} = \sum_i \sum_b A_{ijb} = \sum_i \int A_{ij}(\nu)\mathrm{d}\nu = \sum_i \int A^q_{ij}(\nu)\mathrm{d}\nu. \tag{8}$$

2.5. TOF bin definition

The notion of TOF bin for TOF histogram data is frequently used and straightforward. However, it does not account for the approach (6) for list-mode data with quantized TOF measurements, for the following reasons: this approach is not derived from the TOF histogram equation (3) and it deals with quantization instead of histogramming. In order to provide expressions for TOF weights and estimations of random and scattered coincidences for all types of ML-EM equations using the same formalism, we redefine the term 'TOF bin', so that it refers either to (a) the quantization bin, which only makes individual TOF measurement values less precise, without implying any summing of counts in the raw data, or to (b) the cumulative bin, which implies the accumulation or summing of counts with a certain range of associated TOF measurement values. Hence, the quantization bin is used in (6) and the cumulative bin is used in (3) and (4). The distinction is relevant because the TOF weights and the estimations of expected count rates of random and scattered coincidences have to be computed accordingly. Both types of TOF bin can be represented with a box function Π_b, with width $\Delta\nu_b$, center

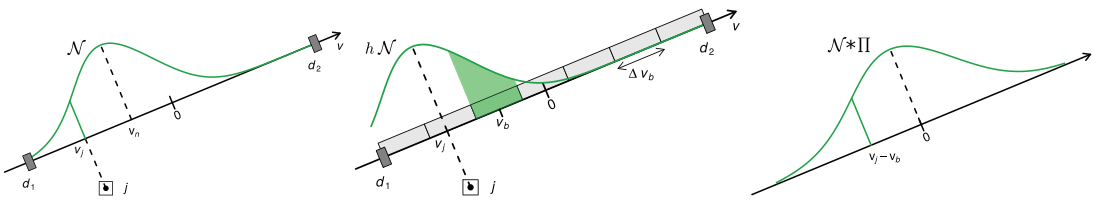

Figure 2. Illustration of the computation of TOF weights for continuous TOF measurements (left), for TOF bins using approach (10*a*) (center) and for TOF bins using approach (10*b*) (right).

v_b, and value h, as (9). The cumulative TOF bin has $h = 1$ and its integral equal to the bin width Δv_b, whereas the quantization TOF bin has $h = 1/\Delta v_b$ and its integral equal to 1.

$$\Pi_b(v) = \begin{cases} h & \text{for } v_b - \Delta v_b/2 < v \leqslant v_b + \Delta v_b/2 \\ 0 & \text{otherwise.} \end{cases} \tag{9}$$

2.6. Computing TOF weights

Here we investigate different approaches to computing the TOF weights, under the assumption of a Gaussian TOF uncertainty model. TOF weights can be expressed from two equivalent points of view: (a) by considering the contribution of each voxel to a TOF bin or measurement, or (b) by considering an uncertainty function associated to a TOF bin or measurement, and sampled for each voxel. Usually, TOF bins are equidistant and have the same width, which simplifies computations greatly.

When computing the TOF weight for a list-mode detected coincidence n with its associated continuous TOF measurement v_n, it is equivalent to (a) center the Gaussian function at the voxel projection onto the LOR v_j and sample it at v_n and (b) center the Gaussian function in v_n and sample it at v_j (see figure 2 left).

TOF weights for TOF bins can be formulated in the same manner for both cumulative (w_{ijb}) and quantization ($w^q_{ij}(v_b)$) bins, based on several approaches:

$$\int \mathcal{N}(v|v_j,\sigma)\Pi(v|v_b,\Delta v_b)\mathrm{d}v = h\int_{v_b-\Delta v_b/2}^{v_b+\Delta v_b/2} \mathcal{N}(v|v_j,\sigma)\mathrm{d}v \tag{10a}$$

$$= \Big(\mathcal{N}(\cdot|0,\sigma) * \Pi(\cdot|0,\Delta v_b)\Big)\Big(v_j - v_b\Big) \tag{10b}$$

$$\approx \mathcal{N}(v_b|v_j,\sigma)h\Delta v_b. \tag{10c}$$

The contribution of a voxel j to a bin b for a LOR can be expressed using (10*a*) (see figure 2 center). This was explicited in Mehranian *et al* (2016) for cumulative TOF bins. Equivalently, it can be expressed by first computing the convolution (10*b*), which is a function of the distance between the TOF bin center and the voxel projection onto the LOR, and then sampling it for the given voxel and TOF bin (see figure 2 right). These two approaches are equivalent in theory, but in practice (10*a*) is more suited for computation on the fly and (10*b*) is more suited for precomputation (slight differences may occur depending on the precision of the precomputed function, see figure 3). It should be noted that the difference between weights for cumulative bins w_{ijb} and for quantization bins $w^q_{ij}(v_b)$ boils down to a single multiplicative factor equal to the TOF bin width: $w^q_{ij}(v_b) = w_{ijb}/\Delta v_b$. Therefore, the two approaches to list-mode reconstruction with quantized TOF measurements (4) and (6) are equivalent, the difference being conceptual.

Various approximations can be used for simplifying computations. TOF quantization bins can be simply neglected, which implies reverting to the continuous list-mode (5). The weights for cumulative TOF bins can be approximated by simple multiplication of a Gaussian sample with the width of the TOF bin (10*c*). This is equivalent to the approach in Lois *et al* (2010), Watson (2007), and in the CASToR version 2, where there is no concern about absolute value: the TOF weights are computed for all TOF bins for a voxel and a LOR, and then normalized by their sum to satisfy the sum consistency (7). Equation (10*c*) is a crude approximation to (10*a*) or (10*b*), and can be viewed as a decrease of the nominal σ. There may be other approximations in between, such as (10*c*) with a larger σ that accounts for the TOF bin width.

The nominal Gaussian function can be truncated, for instance to a certain number of standard deviations. Truncation implies setting some TOF weights and consequently system matrix elements to zero. This impairs the sum consistency (7), which may have the following consequences: (a) if the voxel sensitivity factors are computed using the system matrix with truncation, they will differ from non TOF sensitivity factors and (8) will not be satisfied anymore, (b) if the voxel sensitivity factors are computed using the system matrix without truncation, (8) will be satisfied but discrepancies will occur between the system matrix elements used

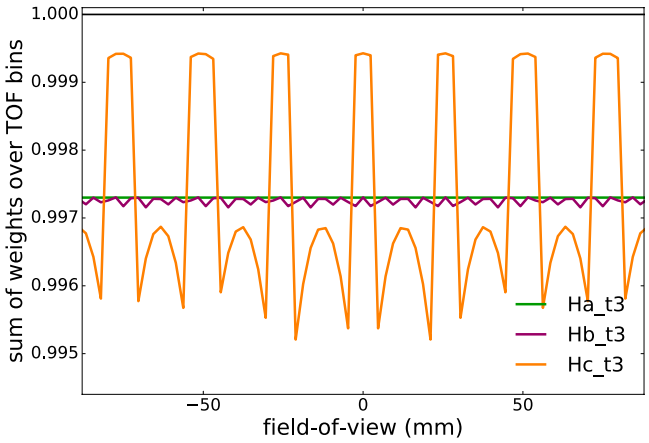

Figure 3. $\sum_b w_{ijb}$ for all voxels j along the horizontal LOR passing through the center of the scanner, for different implementation approaches with truncation of the Gaussian function at 3σ.

for projection/backprojection operations and the voxel sensitivity factors. To ensure that (8) is satisfied, the truncated Gaussian function may be normalized so that its integral equals 1. However, such a function would represent a different TOF uncertainty model with a different standard deviation.

Building the TOF weights independently from the projection component p of the system matrix implies that the TOF component has a constant value over the volume of a single voxel. In theory, it may be more accurate to account for TOF directly in the formulas for computing the projection component of the system matrix p_{ijb} or $p_{ij}(v)$. In this case, a more general sum consistency property must be satisfied: $\sum_b p_{ijb} = p_{ij}$ and $\int p_{ij}(v)\mathrm{d}v = p_{ij}$. However, in practice, this question has not been studied and may become relevant if the TOF uncertainty is reduced to the order of the voxel size.

2.7. Random coincidences

The random coincidences depend on the detection process and their associated TOF measurements may be considered random as well. In view of the sum consistency (1), we want a model (2) such that $\sum_b \bar{r}_{ib} = \bar{r}_i$ and $\int \bar{r}_i(v)\mathrm{d}v = \bar{r}_i$. Let us consider a widespread method for estimating the expected count rate of random coincidences for a LOR i, $\bar{r}_i = S_{i1}S_{i2}2\tau$, where S_{i1} and S_{i2} are the rates of single counts detected at LOR end points, and τ is the timing window for coincidence detection. The expected random count rate per cumulative TOF bin $\bar{r}_{ib}$ can be estimated by replacing 2τ with the temporal size of the TOF bin Δt_b. This is equivalent to dividing the standard estimation $\bar{r}_i$ by the number of TOF bins. This estimation was mentioned in Haynor *et al* (1988), and used for list-mode reconstruction with quantized TOF measurements (4) in Wang *et al* (2006), Zhang *et al* (2017). The continuous expected random count rate $\bar{r}_i(v)$ can be regarded as a limit case when the width of the TOF bin approaches 0. As it is a function of the distance v along the LOR, it can be estimated by dividing the estimation $\bar{r}_i$ with the spatial total span of TOF measurements (∼spatial equivalent of the coincidence timing window), which gives a constant $2S_{i1}S_{i2}/c$. The estimation $\bar{r}_i^q(v_b)$ for quantized TOF measurements in (6) also equals the same constant. Hence, for a LOR, the estimation of the random count rate is the same for all TOF bins, or equivalently for all continuous or quantized TOF measurements.

2.8. Scattered coincidences

The estimation of scattered coincidences must also include the estimation of their associated TOF measurements. Two main methods have been developed for the estimation of the expected count rate of scattered coincidences: Watson (2007) provides scatter estimation $\bar{s}_{ib}$ for cumulative TOF bins and Werner *et al* (2006) provides a continuous scatter estimation $\bar{s}_i(v)$. As for random coincidences, we want a model such that $\sum_b \bar{s}_{ib} = \bar{s}_i$ and $\int \bar{s}_i(v)\mathrm{d}v = \bar{s}_i$. Depending on the availability of estimation methods, the cumulative and quantization bin estimations $\bar{s}_{ib}$ and $\bar{s}_i^q(v_b)$ can be obtained from continuous estimations as

$$h\int_{v_b-\Delta v_b/2}^{v_b+\Delta v_b/2} \bar{s}_i(v)\mathrm{d}v \approx \bar{s}_i(v_b)h\Delta v_b, \tag{11}$$

and continuous estimations can be approximated from cumulative bin estimations as

$$\bar{s}_i(v_b - \Delta v_b/2 \leqslant v < v_b + \Delta v_b/2) \approx \bar{s}_{ib}/\Delta v_b. \tag{12}$$

Table 1. Differences between implementations.

	Hc versus Ha	Ha_t3 versus Ha	Lc versus La	La_t3 versus La
RMSE (%)	∼3	∼0.1	∼0.01	∼0.1
ROI SUV measures (%)	∼−1	∼−0.01	∼−0.001	∼−0.1

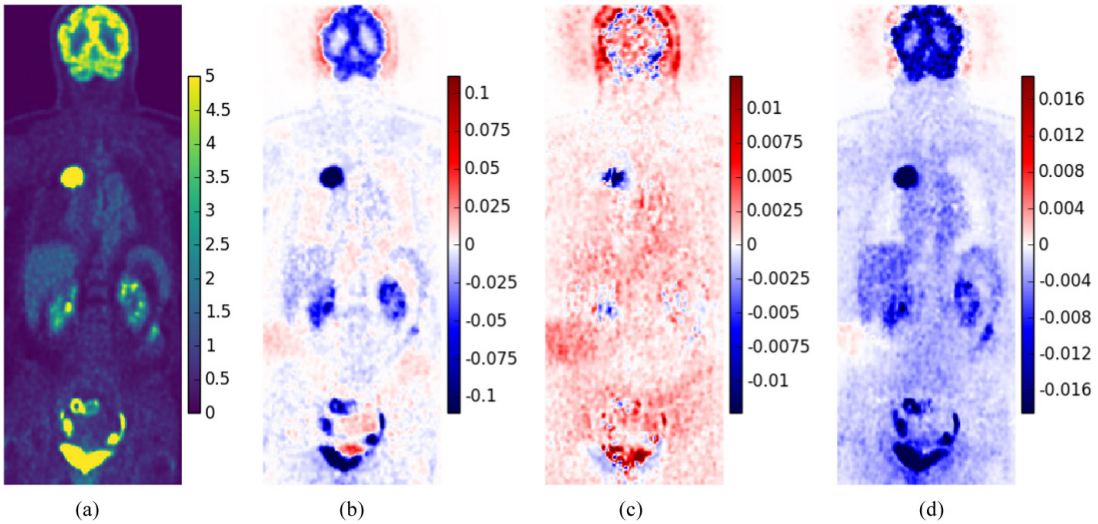

Figure 4. (a) Histogram reference reconstruction Ha, (b) difference image for approximated TOF bins weights (Hc versus Ha), (c) difference image for Gaussian truncation (Ha_t3 versus Ha) and (d) (La_t3 versus La); the unit of color scales is SUV.

3. Comparison of TOF implementations

3.1. Method

All the approaches mentioned in this paper have been implemented in the CASToR platform and will be included in the CASToR version 3. Hence, TOF weights for TOF bins can be computed using (10*a*) (integral computation on the fly using erf), (10*b*) (precomputed convolution sampled on the fly) and (10*c*) (either precomputed function sampled on the fly or computation on the fly using exp). TOF weights for continuous TOF measurements can be computed on the fly or precomputed. The reconstruction of list-mode data with quantized TOF measurements is implemented using (6) only, which is equivalent to (4). The Gaussian distribution can be truncated to a given number of standard deviations σ. Different implementations are referred to as equation $(10)_t$ number of σ for truncation if present, for instance Ha_t3 for histogram reconstruction with (10*a*) and truncation to 3σ.

Whole body scans of two patients with high body mass index (BMI) were selected from the GE Signa PET/MR scanner (GE Healthcare, Milwaukee, WI, USA). The scanner TOF characteristics were: 13.02 ps (1.95 mm) quantization TOF bin, 169.26 ps (25.37 mm) cumulative TOF bin, and 420 ps (62.96 mm) nominal TOF resolution (FWHM). The data were formatted into a TOF histogram and a list-mode with quantized TOF measurements. The reconstruction parameters were similar to parameters in clinical routine: OSEM reconstruction with two iterations and 27 subsets, voxel size $2.34 \times 2.34 \times 2.78$ mm^3, sieve reconstruction with kernel equal to the scanner resolution PSF (Snyder *et al* 1987, Stute and Comtat 2013).

It should be noted that there are differences in computation of voxel sensitivities for different data formats. For list-mode data, sensitivity is precomputed using all the LORs and using system matrix elements without TOF weights, because of (8). Hence, inconsistencies may occur between the sensitivity and the system matrix elements when approximations to TOF weights are used. For histogram data, there are no such inconcistencies because the sensitivity is computed on the fly for each OSEM subset using approximated TOF weights.

We tested all the approaches to the computation of TOF bin weights (10*a*)–(10*c*), without and with Gaussian truncation at 3σ. All the approaches for a data format were compared to the reference approach for that data format, which was (10*a*) without truncation. Differences were evaluated using the root-mean-square error presented as a % of the mean value in the image, using difference images and using SUV quantification in tumoral regions of interest (SUV mean, max, peak).

3.2. Results

Figure 3 shows an illustration of the effect of Gaussian truncation on the sum consistency (7). The implementation Ha_t3 presents a sum lower than 1 (∼0.9973), stable along the LOR. The implementation Hb_t3 presents slight

fluctuations due to the precision of the precomputed convolution (here set to 0.01 mm to make the effect visible), and Hc_t3 presents larger fluctuations due to the approximations.

Here we expose only some noteworthy differences resulting from the comparison of images reconstructed using different implementations. The order of magnitude of differences is presented in table 1 and relevant images of differences are presented in figure 4.

For histogram data, the approximation of (cumulative) TOF bin weights (Hc versus Ha) resulted in the largest differences and in contrast loss (see figure 4(b)). Truncating the Gaussian (Ha_t3 versus Ha) produced lower differences, partially due to the fact that the sensitivity is consistent with the computed truncated TOF weights. For list-mode data, the approximation of (quantization) TOF bins (Lc versus La) produced the same effect as for histogram data, but with much lower differences, because the TOF bin is one order of magnitude smaller. Truncating the Gaussian (La_t3 versus La) resulted in comparatively larger differences and in a general loss of intensity (see figure 4(d)), due to the inconsistencies between the voxel sensitivity and the computed truncated TOF weights.

Direct comparison between the histogram and the list-mode reconstruction is not shown, because the difference depends on several factors, not necessarily related to TOF. In order to perform a fair comparison, the number of subsets should be 1, the voxel sensitivity factors strictly identical, the TOF bin identical, and (4) used for list-mode reconstruction. The main reason for using approximations is reducing the implementation complexity and the computation time. These depend strongly on the software framework and on computer architecture. In CASToR implementation, the approximations do accelerate computations up to a factor of 4, but a detailed analysis of computation time was not an aim of this paper. For the scanner and setup used in this study, the order of magnitude of differences between implementations (less than a couple of percents) is not larger than the order of magnitude of typical bias in standard clinical OSEM reconstructions (Schöder *et al* 2004). The differences are in accordance with the presented theoretical and practical implementation details.

4. Conclusion

We provide theoretical and practical details for implementing TOF in PET reconstruction. Several approaches have been implemented in the CASToR platform and shall be available in the next release (version 3). The differences between approaches are shown to be of low importance for standard reconstructions of clinical data.

Acknowledgments

This work is supported by the Lidex-PIM project funded by the IDEX Paris-Saclay (ANR-11-IDEX-0003-02), by the French national research agency (ANR-16-CE17-0011-001), and by the 'MMIPROB' project funded by ITMO Cancer (France). Thanks to Antoine Pierucci for drawing the diagrams in figure 2 and thanks to Maxime Toussaint for the encouragement.

References

CAS 2017 Castor—customizable and advanced software for tomographic reconstruction (www.castor-project.org/)

Clementel E, Mollet P and Vandenberghe S 2013 Effect of local TOF Kernel miscalibrations on contrast-noise in TOF PET *IEEE Trans. Nucl. Sci.* **60** 1578–88

Daube-Witherspoon M E, Surti S, Matej S, Werner M, Jayanthi S and Karp J S 2006 Influence of time-of-flight Kernel accuracy in TOF-PET reconstruction *IEEE Nuclear Science Symp. Conf. Record* 3, pp 1723–7

Groiselle C J and Glick S J 2004 3D PET list-mode iterative reconstruction using time-of-flight information *IEEE Symp. Conf. Record Nuclear Science* 4, pp 2633–8

Haynor D R, Harrison R L and Lewellen T K 1988 A scheme for accidental coincidence correction in time-of-flight positron tomography: theory and implementation *IEEE Trans. Nucl. Sci.* **35** 753–6

Levin C S, Maramraju S H, Khalighi M M, Deller T W, Delso G and Jansen F 2016 Design features and mutual compatibility studies of the time-of-flight pet capable ge signa PET/MR system *IEEE Trans. Med. Imaging* **35** 1907–14

Lois C, Jakoby B W, Long M J, Hubner K F, Barker D W, Casey M E, Conti M, Panin V Y, Kadrmas D J and Townsend D W 2010 An assessment of the impact of incorporating time-of-flight information into clinical PET/CT imaging *J. Nucl. Med.* **51** 237–45

Matej S, Surti S, Jayanthi S, Daube-Witherspoon M E, Lewitt R M and Karp J S 2009 Efficient 3D TOF PET reconstruction using view-grouped histo-images: direct–direct image reconstruction for TOF *IEEE Trans. Med. Imaging* **28** 739–51

Mehranian A, Kotasidis F and Zaidi H 2016 Accelerated time-of-flight (TOF) PET image reconstruction using TOF bin subsetization and TOF weighting matrix pre-computation *Phys. Med. Biol.* **61** 1309

Merlin T, Stute S, Benoit D, Bert J, Carlier T, Comtat C, Filipovic M, Lamare F and Visvikis D 2018 Castor: a generic data organization and processing code framework for multi-modal and multi-dimensional tomographic reconstruction *Phys. Med. Biol.* **63** 185005

Schöder H, Erdi Y E, Chao K, Gonen M, Larson S M and Yeung H W 2004 Clinical implications of different image reconstruction parameters for interpretation of whole-body pet studies in cancer patients *J. Nucl. Med.* **45** 559–66

Snyder D L and Politte D G 1983 Image reconstruction from list-mode data in an emission tomography system having time-of-flight measurements *IEEE Trans. Nucl. Sci.* **30** 1843–9

Snyder D L, Miller M I, Thomas L J and Politte D G 1987 Noise and edge artifacts in maximum-likelihood reconstructions for emission tomography *IEEE Trans. Med. Imaging* **6** 228–38
Stute S and Comtat C 2013 Practical considerations for image-based PSF and blobs reconstruction in PET *Phys. Med. Biol.* **58** 3849–70
Wang W *et al* 2006 Systematic and distributed time-of-flight list mode PET reconstruction *IEEE Nuclear Science Symp. Conf. Record* 3, pp 1715–22
Watson C 2007 Extension of single scatter simulation to scatter correction of time-of-flight PET *IEEE Trans. Nucl. Sci.* **54** 1679–86
Werner M E, Surti S and Karp J S 2006 Implementation and evaluation of a 3D PET single scatter simulation with TOF modeling *IEEE Nuclear Science Symp. Conf. Record* 3 pp 1768–73
Zhang X, Zhou J, Cherry S R, Badawi R D and Qi J 2017 Quantitative image reconstruction for total-body PET imaging using the 2 m long EXPLORER scanner *Phys. Med. Biol.* **62** 2465–85